Performances Analysis of a Micro-Grid Connected Multi-Renewable Energy Sources System Associated with Hydrogen Storage

Salah Tamalouzt, Nabil Benyahia, Abdelmounaïm Tounzi, Amar Bousbaine

Chapter 24

Performances Analysis of a Micro-Grid Connected Multi-Renewable Energy Sources System Associated with Hydrogen Storage

Salah Tamalouzt, Nabil Benyahia, Abdelmounaim Tounzi and Amar Bousbaine

Abstract

This work highlights the modeling and simulation of a micro-grid connected renewable energy system. It comprises of wind turbine (WT) based on doubly fed induction generator (DFIG), photovoltaic generator (PV), fuel cell (FC) generator, a Hydrogen tank, a water electrolyzer used for long-term storage, and a battery bank energy storage system (BBESS) utilized for short-term storage. In this paper, a global control strategy and an energy management strategy are proposed for the overall system. This strategy consists in charging the BBESS and producing hydrogen from the water electrolyzer in case of power excess provided from WT-DFIG and photovoltaic generators. Therefore, the FC and the BBESS will be used as a backup generator to supply the demand required power, when the WT-DFIGs and the PV energy are deficient. The effectiveness of this contribution is verified through computer simulations under Matlab/Simulink, where very satisfactory results are obtained.

Keywords: AC and DC micro-grid applications, multi-renewable energy sources, energy management system, hybrid energy storage system, hydrogen production and storage, doubly fed induction generator, direct active and reactive powers control, local reactive energy compensator

1. Introduction

A growing interest in renewable energy resources (RESs) has been observed these last years. The alternative energy sources (AESs) are non-polluting, free in their availability and continuous. These advantages make this type of energy attractive in remote locations and for microgrid applications [1, 2]. To experience the best benefits of these sources, many energy sources can be used for hybrid energy generators systems, including wind turbine (WT), Hydro-electric power (HEP), photovoltaic panels (PV), Fuel Cells (FC) and micro-turbines [1–38]. Nevertheless, the major RESs used and reported in the literature are WT and PV [1–33].

Indeed, a high RESs penetration can be created reliability, power quality and stability problems in the main electrical grid. We must think of more effective solutions to remedy these problems. For these, the microgrid (MG) is one of the solutions. In addition, for efficient and economical utilization of these RESs, some forms of backup systems are almost universally required. In the case these RESs are based on WTs or PVs, then Energy Storage Systems (ESSs) are necessary to further mitigate the effects of the seasonal and daily randomness fluctuations in the climatic (solar radiation, wind speed, temperature) and geographical conditions as well as the profiles of the required power. In addition, to maintain the power and energy balance as well as to improve the output power quality [2–6].

To ensure proper operation of the ESSs, they must have a high-power density in order to face fast power variations, and at the same time, they must have a high energy density to give autonomy to the MG. For these reasons, it is necessary to associate more than one storage technology creating a Hybrid Energy Storage Systems (HESSs). Knowing that the energy storage system as battery banks (BBs) is very important for the efficient and economical utilization of the MG system [25]. However, the lifetime of these systems decreases according to their operating modes, particularly according charge and discharge cycles [5, 6, 37]. To improve the energy supply reliability of WTs and PVs hybrid system, a fuel cell (FC) can be combined with an electrolyzer system, thus constituting a third energy source, to ensure the need for any additional, backups or supply power system [26].

Thus, the fuel cell (FC) and electrolyzer technology ideally fulfill the need for any backups the supply power system, and hydrogen is a suitable option and it can be used as a fuel to get a reliable power for almost every application that used fossil fuels [3, 38]. The coupling of the differents energy sources, using a combination of the WT, PV array, FC with electrolyzer containing a BBESS is one of the most efficient procedures to produce very high-quality energy [2, 3, 38]. This configuration brings us to speak of an electrical MG, which is associated with distributed generation and decentralized management, directed at developing small electrical grids that are normally connected to the general electricity grid. The associated energy storage devices make possible to balance out the power exchange between the MG supply and demand, and also between the MG and the grid [3].

Several studies and various configurations of an hybrid micro-grid applications-based WTs and PVs generations have been proposed in the litterature [1–33]. However, a little attention has been given for the integration of a DFIG on the MG system. Indeed, the DFIG driven by wind turbine (WT-DFIG) brings more benefits to the wind energy conversion system such as direct access on the AC grid, the reactive power compensation unit is not needed, the ability of opertating at three modes (sub, super and synchronous mode including the over-speed mode), the capability of producing electric power more than the rated power and a flexible active and reactive power control. Furthermore, the size of the AC/AC frequency converter with its DC-bus capacitor, the rotor side controller, the converter costs and power losses are reduced [2–6].

The power converter with its control and protection are the key of the DFIG advantages for electrical grid integration. Knowing that the variable speed constant frequency operation of DFIG can be realized by adjusting the amplitude, frequency, phase and phase sequence. If an appropriate control strategy is adopted, active and reactive powers of the DFIG can be regulated independently, which makes this machine as an active energy production system and a local reactive energy compensator. The AC excitation performance has a direct influence on the WT-DFIG operation. In the aim to develop efficient and economical wind energy conversion systems, different algorithm control applied to WT-DFIG have been proposed in the literature [2–23]. Conventional control strategies are generally based on two

most families, which are; the direct control techniques namely the direct torque control or the direct power control (DPC) [2–16], and indirect control strategies based on field-oriented control (FOC) [17–23]. In this case, we have the FOC Linear Vector Control (FOC-LVC) methods [17, 18] and the FOC non-linear Vector Control (FOC-NLVC) [19–23], which are have been widely applied to WT-DFIG in differents operating quadrants and modes in many research works. The variable-structure control technique based on sliding mode control (SMC), is the most widely used nonlinear control technique applied to wind turbine control, due to these advantages over other nonlinear techniques [19–21].

Indeed, the advantage of the proposed micro-grid topology is the easier accessibility to AC and DC grid. However, the AC/DC and DC/DC converters required for supplying the DC loads are not needed. So, the main objectives of this contribution are: achieving an optimal and efficient control of the coordination between the different sources; WT-DFIG, PV and FC, BBESS and electrolyzer, ensuring better power quality for customers (for DC or AC grid) and regulating the output voltage amplitude and frequency (AC grid voltage). Moreover, to ensure continuity of service (provide the output energy needed) and a local reactive power compensation, while operating maximum use of benefits of the proposed topology, even in extreme operation conditions. In addition, the micro-grid based on the multi-source topology can increase the flexibility of grid connection power management and vice versa. Indeed, assessing the usefulness of the proposed system depends on the applied system-control effectiveness, in particular the active and reactive power control of the DFIG, and the applied management algorithm in very severe situations (change in power demand, the random variations and sudden conditions of meteorological, ensure continuity of service, ...).

This work focuses on the development of simulation model to design and analyze the micro-grid system overall performances. A combination of the WT-DFIG, PV array, BBESS, and FC-electrolyzer is used. The numerical simulation model is used not only to analyzing hybrid system performances, but also for designing this last one, to meet for all load demands for any available meteorological condition. For this, the simulation of applied management algorithm of the whole system in very severe situations, such as a change in power demand random variations and sudden meteorological conditions, is presented and the results are discussed.

The paper is summarized as follows: In Section 2, a brief description of the proposed micro-grid is presented. In Section 3, a DRPC principle applied to the WT-DFIG, and the reactive power local compensation system sought is explained. Unit sizing of wind generation, PV, electrolyzer, and FC are given in this section. In addition, the control strategy is developed to regulate the voltage and hence coordination among sources, storages (battery bank and electrolyzer) is explained. The detailed simulation results of the different situations studied with their comments are presented in Section 4. Finally, the main paper conclusions are given.

2. Description of the proposed micro-grid

The proposed hybrid energy system, shown in **Figure 1**, consists of a Doubly Fed Induction Generator (DFIG) based variable speed wind energy conversion, PV array, battery bank, fuel cell, and electrolyzer. The primary sources, wind speed turbine and PV, are connected to the common DC-grid and equipped with optimum powers algorithms extracting. For the PV generator, the maximum power point tracking (MPPT) is applied, whereas, in the WT source case, it depending on the operating zone of the WT, MPPT technique and pitch angle control are considered to optimize the wind energy efficiency. BBESS is used as a storage device and is

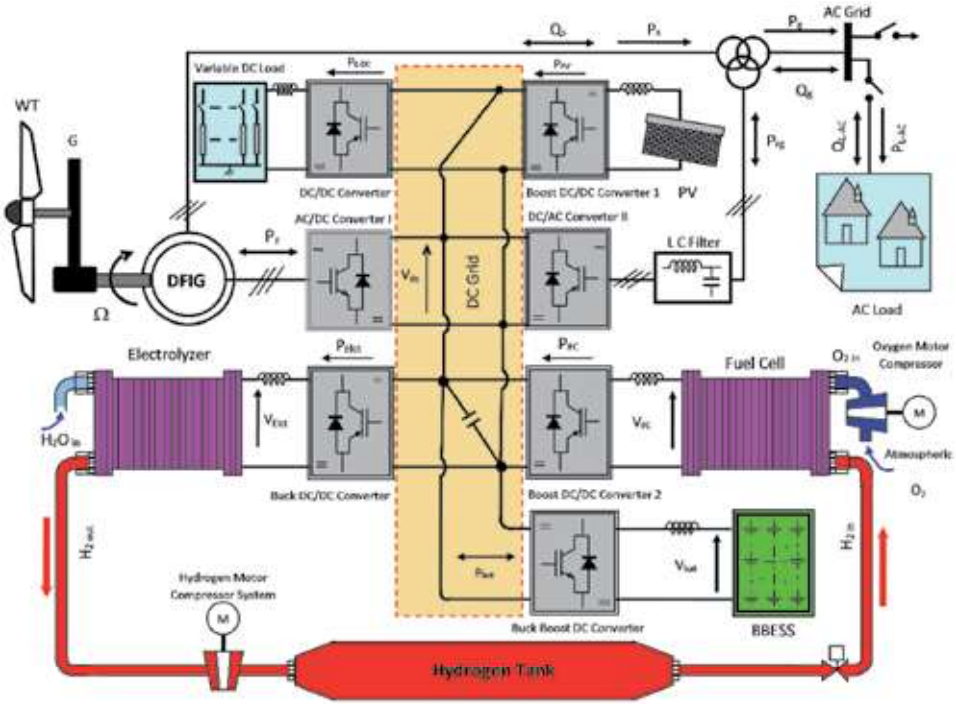

Figure 1.
Global control scheme combining RESs (WT-DFIG with PV) with HESS associated with hydrogen energy production (HEP).

connected to DC-grid through DC/DC buck-boost converter (BBDC). Wind and solar powers depend on weather conditions and during night hours solar power is zero. Therefore, under the situation of long-term no-wind and solar or low-wind and solar condition, the BBESS alone cannot cater to the load demand. Hence, fuel cell (FC) is integrated to make the system more sustainable.

In case of high-power generation from wind and solar for a long time and the BBESS hits its upper limit of charge-storage, the electrolyzer comes into effect and consumes the surplus power, while generating hydrogen. This hydrogen produced from the electrolyzer is stored in the tanks, where can be used as input to supply the FC.

3. Modeling and control of the proposed micro-grid

3.1 Modeling and control of the wind energy conversion system

3.1.1 Wind energy conversion system modeling

The wind turbine mathematical model consists of the modeling of its aerodynamic torque T_t which is given by the following relation [3, 10]:

$$T_t = \frac{1}{2} C_p \frac{\rho \pi R^2}{\Omega_t} \nu^3 \quad (1)$$

where, ν, ρ and R are respectively the wind speed, the air density and the rotor radius. Besides, Ω_t and C_p are the turbine speed and the power coefficient. The tip-speed ration (λ) is given by the Eq. (3) [3, 10]:

$$\lambda = \frac{\Omega_t \cdot R}{\nu} \tag{2}$$

Figure 2 shows the wind turbine characteristic, where, in the region (I) (MPPT control region), the tip speed ratio is maintained at its optimal value $\lambda_{opt} = 9$ and the power coefficient is always maintained at its maximum value ($C_{pmax} = 0.49$). In this case, the reference electromagnetic torque applied as being an input to the proposed DFIG control in the control is given by:

$$T_{em\ ref} = \frac{1}{2} C_{p-max} \frac{\rho \pi R^5}{G^3 \lambda_{opt}^3} \nu^3 \tag{3}$$

In the regions (II) and (III), called Pitch angle control regions, the generated active power is maintained constant. The power coefficient (C_p) for wind turbine model is given as a function of tip-speed ratio (λ) and the blade pitch angle (β). In this work, the following expression is used [2, 3, 10]:

$$\begin{aligned} C_p(\lambda, \beta) = 0.5176 \cdot [116 \cdot (1/\lambda_i) - 0.4 \cdot \beta - 5] \\ \exp(-21/\lambda_i) + 0.0068 \cdot \lambda_i \end{aligned} \tag{4}$$

with: $\frac{1}{\lambda_i} = \frac{1}{\lambda + 0.08 \cdot \beta} - \frac{0.035}{1+\beta^3}$.

3.1.2 Control of wind turbine generator (WT-DFIG)

When the DFIG is connected to an existing AC grid, as shown in **Figure 1**, this connection must be established in the following done in three steps. The first step is the stator voltages regulation with the AC grid voltages as reference synchronization. The second step is the stator connection to this grid. As the voltages of the two devices are synchronized, the connection can be effectively established. Once this connection is achieved, the third step is the regulation of the transit of the power between the DFIG and the AC grid.

In this work, the WT-DFIG control is based on the control of the exchanged powers between the AC-grid and the WT-DFIG. To provide independent control of the active power P_g and reactive power Q_g exchange between the AC-grid and WT-DFIG, by means of rotor voltage regulation, it is necessary to define the dq

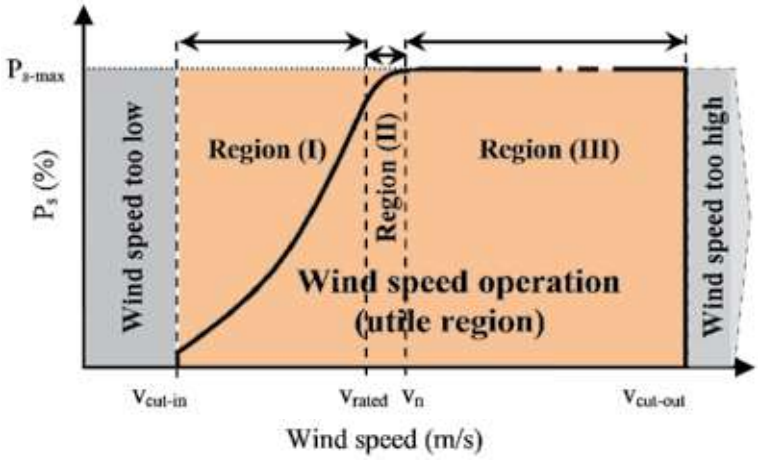

Figure 2.
Operation regions of wind turbine.

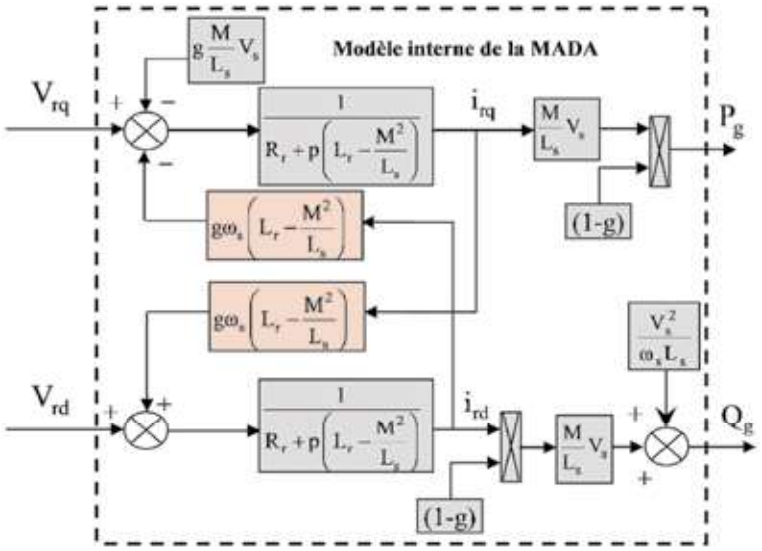

Figure 3.
Simplified scheme model of DFIG.

components of the rotor voltages in the stator-flux oriented reference frame and show that P_g and Q_g can be represented as functions of the individual voltage components. Subsequently, the P_g and Q_g control can be used to determine the reference rotor voltages.

The AC grid active and reactive powers are directly controlled, assuming that the optimal mechanical power developed by the turbine is known, as shown in **Figure 2**. The reference AC grid active and reactive powers, denoted by (P_g^*, Q_g^*) are used as the reference value for the WT-DFIG power control loop. In the inner voltage control loop, the method of stator flux oriented vector control, combining with the Variable structure control (VSC) possesses based on the nonlinear SMC is applied. They are used to establish a reference frame, that allows the d and q axis components of the rotor voltage to be controlled independently. Adjustment of the q-axis component of the rotor voltage, V_{qr}, controls the developed generator torque or the AC grid-side active power of the WT-DFIG (P_g). Regulating the d-axis component, V_{dr}, controls directly the grid-side reactive power flow (Q_g), as illustrated in **Figure 3**.

The two-phase model of the Doubly Fed Induction Machine (DFIM) expressed in the rotor frame is used. The classical electrical equations are written in this frame, as follows [3]:

$$\begin{cases} \dfrac{di_{sd}}{dt} = \dfrac{1}{L_s}\left[V_{sd} - M\dfrac{di_{rd}}{dt} - R_s i_{sd} + \omega_s L_s i_{sq} + \omega_s M i_{rq}\right] \\ \dfrac{di_{sq}}{dt} = \dfrac{1}{L_s}\left[V_{sq} - M\dfrac{di_{rq}}{dt} - R_s i_{sq} - \omega_s L_s i_{sd} - \omega_s M i_{rd}\right] \\ \dfrac{di_{rd}}{dt} = \dfrac{1}{L_r}\left[V_{rd} - M\dfrac{di_{sd}}{dt} - R_r i_{rd} - (\omega_s - \omega) L_r i_{rq} - (\omega_s - \omega) M i_{sq}\right] \\ \dfrac{di_{rq}}{dt} = \dfrac{1}{L_r}\left[V_{rq} - M\dfrac{di_{sq}}{dt} - R_r i_{rq} + (\omega_s - \omega) L_r i_{rd} + (\omega_s - \omega) M i_{sd}\right] \end{cases} \quad (5)$$

with: $\begin{cases} L_s = l_s + M \\ L_r = l_r + M \end{cases}$.

where R_s, R_r, l_s and l_r are the phase resistances and leakage inductances respectively. The M represents the magnetizing inductance, Ω is the mechanical speed and

p the pair pole number. Besides, v_{sd}, v_{sq}, i_{sd} and i_{sq} are the d-q stator voltage and currents, respectively. While the v_{rd}, v_{rq}, i_{rd} and i_{rq} are the rotor voltage and currents, along the d-q axis, respectively.

The vector control strategy, using the Park transformation, allows to decoupling the control of active and reactive powers [3, 19]. By setting the stator flux vector aligned with d-axis, we have:

$$\begin{cases} \psi_{ds} = \psi_s = L_s i_{ds} + M i_{qs} \\ \text{and} \\ \psi_{qs} = L_s i_{qs} + M i_{ds} = 0 \end{cases} \tag{6}$$

The electrical active and reactive powers at the rotor, delivered by the stator as well as those provided for the AC grid are defined as:

$$\begin{cases} P_s = v_{ds} i_{ds} + v_{qs} i_{qs} \\ Q_s = v_{qs} i_{ds} - v_{ds} i_{qs} \end{cases} \tag{7}$$

$$\begin{cases} P_r = v_{dr} i_{dr} + v_{qr} i_{qr} \\ Q_r = v_{qr} i_{dr} - v_{dr} i_{qr} \end{cases} \tag{8}$$

$$\begin{cases} P_g = P_s + P_r \\ Q_g = Q_s + Q_r \end{cases} \tag{9}$$

The electromagnetic torque is defined as follows:

$$T_{em} = p\left(\psi_{ds} i_{qs} - \psi_{qs} i_{ds}\right) \tag{10}$$

$$T_{em} = p\frac{L_s}{M}\left(\psi_{ds} i_{qs}\right) \tag{11}$$

The electromagnetic torque and then the active power are controlled through the q-axis rotor current and d-axis rotor current control the reactive power. Neglecting the phase stator resistance R_s (that's the case of medium power machines used in wind energy conversion systems). In order to calculate Park transformation angles for the stator and rotor variables, the stator pulsation and the mechanical speed must be sensed. By choosing this reference frame, stator voltages and fluxes can be rewritten as follows:

$$\begin{cases} v_{ds} = 0 \\ \text{and} \\ v_{qs} = v_s = \omega_s \psi_{ds} \end{cases} \tag{12}$$

With these relations, as given in Eq. (12), the rotor fluxes, the stator active and reactive power and voltages can be written versus rotor currents as:

$$\begin{cases} \psi_{dr} = \sigma_r\, i_{dr} + \dfrac{M}{\omega_s L_s} v_s \\ \psi_{qr} = \sigma_r\, i_{qr} \end{cases} \tag{13}$$

where, $\sigma_r = L_r\left(1 - \frac{M^2}{L_r L_s}\right)$ and $s = \frac{\omega_r}{\omega_s}$;

The AC grid active power reference to be injected into the AC-grid is determined by multiplying the value of the efficiency (η) of the DFIG by the optimal turbine mechanical power. The latter is sought by the optimization algorithm: The MPPT

technique and pitch angle control are considered to optimize the wind energy efficiency. In addition, The generator mechanical speed remains at its optimum.

$$P_{g\_ref} = \eta\left(-P_{mec\_opt}\right) \tag{14}$$

$$\Omega_{ref} = \Omega_{opt} \tag{15}$$

The AC-grid reactive power reference is determined according to the reactive energy that it is desired to compensate locally.

The DFIG efficiency η is estimated at 96%, knowing that the machine mechanical losses are neglected and static power converters are considered ideal [3, 18].

We first recall the expressions of powers, active and reactive, exchanged with the AC-grid, as well as the rotor currents in the Park coordinate system with stator flux orientation, as given in Eqs. (18) and (20).

$$\begin{cases} P_s = -v_s \dfrac{M}{L_s} i_{qr} \\ Q_s = \dfrac{v_s \psi_{ds}}{L_s} - \dfrac{v_s M}{L_s} i_{dr} \end{cases} \tag{16}$$

$$\begin{cases} v_{dr} = R_r i_{dr} + \sigma_r \dfrac{d}{dt} i_{dr} \text{-} s\omega_s \sigma_r i_{qr} \\ v_{qr} = R_r i_{qr} + \sigma_r \dfrac{d}{dt} i_{qr} \text{-} s\omega_s \sigma_r i_{dr} + s\omega_s \dfrac{L_m}{\omega_s L_s} v_s \end{cases} \tag{17}$$

For relatively weak slip values, Eq. (9) can be simplified by Eq. (18):

$$\begin{cases} P_g = (s-1)\, v_s \dfrac{M}{L_s} i_{qr} \\ Q_g = \dfrac{v_s^2}{\omega_s L_s} + (s-1)\, v_s \dfrac{M}{L_s} i_{dr} \end{cases} \tag{18}$$

$$\begin{cases} \dfrac{di_{rd}}{dt} = \dfrac{1}{\sigma_r}\left(V_{rd} - R_r i_{rd} + \sigma_r \cdot (\omega_s - \omega) \cdot i_{rq} - \dfrac{M}{L_s}\dfrac{d\Phi_s}{dt}\right) \\ \dfrac{di_{rq}}{dt} = \dfrac{1}{\sigma_r}\left(V_{rq} - R_r i_{rq} - \sigma_r \cdot (\omega_s - \omega) \cdot i_{rd} - (\omega_s - \omega) \cdot \dfrac{M}{L_s}\Phi_s\right) \end{cases} \tag{19}$$

$$\Rightarrow \begin{cases} \dfrac{di_{rd}}{dt} = \dfrac{1}{\sigma_r}\left(V_{rd} - R_r i_{rd} + \sigma_r \cdot g \cdot \omega_s \cdot i_{rq}\right) \\ \dfrac{di_{rq}}{dt} = \dfrac{1}{\sigma_r}\left(V_{rq} - R_r i_{rq} - \sigma_r \cdot g \cdot \omega_s \cdot i_{rd} - g \cdot \dfrac{M}{L_s} V_s\right) \end{cases} \tag{20}$$

3.1.2.1 AC-grid active power control

The grid active power surface is given as follow:

$$S(P) = P_{g\_ref} - P_g \tag{21}$$

The derivative of the grid active power surface:

$$\dot{S}(P) = \dot{P}_{g\_ref} - \dot{P}_g \tag{22}$$

$$\Rightarrow \dot{S}(P) = \dot{P}_{g\_ref} - \left((g-1) \cdot V_s \cdot \frac{M}{L_s}\right) \cdot \dot{i}_{rq} \tag{23}$$

We replace the currents of Eq. (20) in Eq. (23), gives us:

$$\dot{S}(P) = \dot{P}_{g\_ref} - (g-1)\cdot V_s \cdot \frac{M}{L_s}\cdot\frac{1}{\sigma_r}\left(V_{rq} - R_r\cdot i_{rq} - \sigma_r \cdot g\cdot \omega_s \cdot i_{rd} - g\cdot\frac{M}{L_s}\cdot V_s\right) \quad (24)$$

We have;

$$V_{rq} = V_{rq(eq)} + V_{rq(n)} \quad (25)$$

Then;

$$\begin{aligned}\dot{S}(P) = \dot{P}_{g\_ref} - (g-1)\cdot V_s \cdot \frac{M}{L_s}\cdot\frac{1}{\sigma_r}\Big(&V_{rq(eq)} + \\ &V_{rq(n)} - R_r\cdot i_{rq} - \sigma_r\cdot g\cdot\omega_s\cdot i_{rd} - g\cdot\frac{M}{L_s}\cdot V_s\Big)\end{aligned} \quad (26)$$

During the slip mode and steady-state, we have:

$$S(P) = 0; \dot{S}(P) = 0; V_{rq(n)} = 0 \quad (27)$$

$$\Rightarrow \begin{cases} V_{rq(eq)} = -\left(\frac{L_s}{M}\cdot\frac{\sigma_1}{(1-g)\cdot V_s}\right)\dot{P}_{g\_ref} + R_r\cdot i_{rq} + \sigma_r\cdot g\cdot\omega_s\cdot i_{rd} + g\cdot\frac{M}{L_s}\cdot V_s \\ V_{rq(n)} = K_{rq}\cdot Sat(S(P)) \\ \\ K_{rq} > 0 \end{cases} \quad (28)$$

The convergence condition is $S(P)\cdot\dot{S}(P) < 0$, is ensured if:

1. $S(P) > 0; \dot{S}(P) < 0$, then:

$$K_{rq} > \left(\left(\frac{L_s}{M}\cdot\frac{\sigma_r}{(g-1)\cdot V_s}\right)\dot{P}_{g\_ref} + R_r\cdot i_{rq} + \sigma_r\cdot g\cdot\omega_s\cdot i_{rd} + g\cdot\frac{M\cdot V_s}{L_s}\right) \quad (29)$$

2. Or $S(P) < 0; \dot{S}(P) > 0$, then:

$$K_{rq} > -\left(\left(\frac{L_s}{M}\cdot\frac{\sigma_r}{(g-1)\cdot V_s}\right)\dot{P}_{g\_ref} + R_r\cdot i_{rq} + \sigma_r\cdot g\cdot\omega_s\cdot i_{rd} + g\cdot\frac{M\cdot V_s}{L_s}\right) \quad (30)$$

From Eqs. (29) and (30), we deduce the K_{rq}:

$$K_{rq} > \left|-\left(\left(\frac{L_s}{M}\cdot\frac{\sigma_r}{(g-1)\cdot V_s}\right)\dot{P}_{g\_ref} + R_r\cdot i_{rq} + \sigma_r\cdot g\cdot\omega_s\cdot i_{rd} + g\cdot\frac{M\cdot V_s}{L_s}\right)\right| \quad (31)$$

3.1.2.2 AC-grid réactive power control

The grid réactive power surface is given as follow:

$$S(Q) = Q_{g\_ref} - Q_g \quad (32)$$

The derivative of the grid active power surface:

$$\dot{S}(Q) = \dot{Q}_{g\_ref} - \dot{Q}_g \quad (33)$$

$$\Rightarrow \dot{S}(Q) = \dot{Q}_{g\_ref} - \left((g-1)\cdot V_s \cdot \frac{M}{L_s}\right)\cdot \dot{i}_{rd} \tag{34}$$

We replace the currents of Eq. (20) in Eq. (34), gives us:

$$\dot{S}(Q) = \dot{Q}_{g\_ref} - (g-1)\cdot V_s \cdot \frac{M}{L_s}\cdot\frac{1}{\sigma_r}\left(V_{rd} - R_r i_{rd} + \sigma_r \cdot g \cdot \omega_s \cdot i_{rq}\right) \tag{35}$$

where;

$$\dot{S}(Q) = \dot{Q}_{g\_ref} - (g-1)\cdot V_s \cdot \frac{M}{L_s}\cdot\frac{1}{\sigma_r}\left(V_{rd(eq)} + V_{rd(n)} - R_r i_{rd} + \sigma_r \cdot g \cdot \omega_s \cdot i_{rq}\right) \tag{36}$$

During the slip mode and steady-state, we have:

$$S(Q) = 0; \dot{S}(Q) = 0; V_{rd(n)} = 0 \tag{37}$$

$$\Rightarrow \begin{cases} V_{rd(eq)} = -\left(\frac{L_s}{M}\cdot\frac{\sigma_r}{(1-g)\cdot V_s}\right)\dot{Q}_{g\_ref} + R_r \cdot i_{rd} - \sigma_r \cdot g \cdot \omega_s \cdot i_{rq} \\ V_{rd(n)} = K_{rd} \cdot Sat(S(Q)) \\ \\ K_{rd} > 0 \end{cases} \tag{38}$$

The convergence condition is $S(Q)\cdot\dot{S}(Q) < 0$, is ensured if:

1. $S(Q) > 0; \dot{S}(Q) < 0$, then:

$$K_{rd} > \left(\left(\frac{L_s}{M}\cdot\frac{\sigma_r}{(g-1)\cdot V_s}\right)\dot{Q}_{g\_ref} + R_r \cdot i_{rd} - \sigma_r \cdot g \cdot \omega_s \cdot i_{rq}\right) \tag{39}$$

2. Or $S(Q) < 0; \dot{S}(Q) > 0$, then:

$$K_{rd} > -\left(\left(\frac{L_s}{M}\cdot\frac{\sigma_r}{(g-1)\cdot V_s}\right)\dot{Q}_{g\_ref} + R_r \cdot i_{rd} - \sigma_r \cdot g \cdot \omega_s \cdot i_{rq}\right) \tag{40}$$

From Eqs. (39) and (40), we deduce the K_{rd}:

$$K_{rd} > \left|-\left(\left(\frac{L_s}{M}\cdot\frac{\sigma_r}{(g-1)\cdot V_s}\right)\dot{Q}_{g\_ref} + R_r \cdot i_{rd} - \sigma_r \cdot g \cdot \omega_s \cdot i_{rq}\right)\right| \tag{41}$$

The schematic diagram of the AC grid active and reactive powers sliding mode control structure, denominated DRPC, is illustrated in **Figure 4**.

3.2 Photovoltaic system modeling and control

The PV cell mathematical model description is represented in [3, 31, 33], where the typical PV module power characteristic is given in [3, 33]. In order to extract the optimum power of the PV array, it is necessary to use an algorithm to operate the

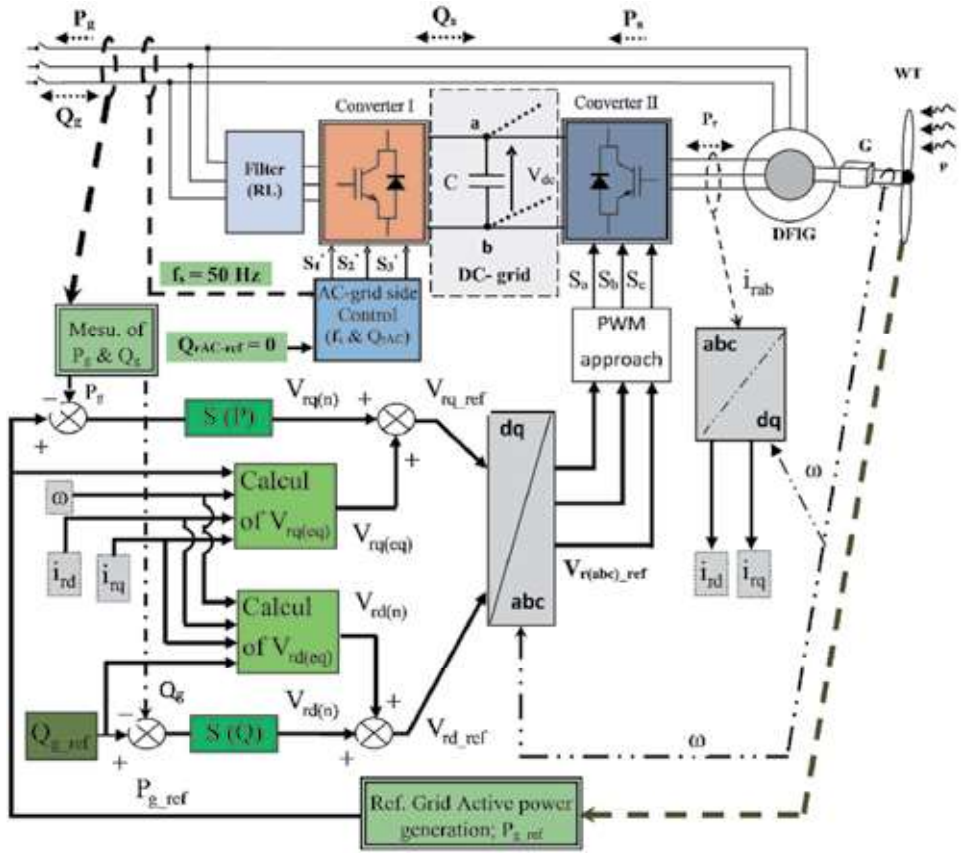

Figure 4.
Schematic diagram of the AC grid active and reactive powers, exchanged with the proposed micro-grid, SMC structure.

PV generator at its maximum power point, called MPPT technique. The MPPT device is a high-frequency boost DC/DC converter (BDCC) inserted between the PV array and the DC-grid, and it takes the DC input from the PV array, convert it to a different DC voltage and current to exactly match the PV array to the DC-grid, as illustrated in **Figure 5**.

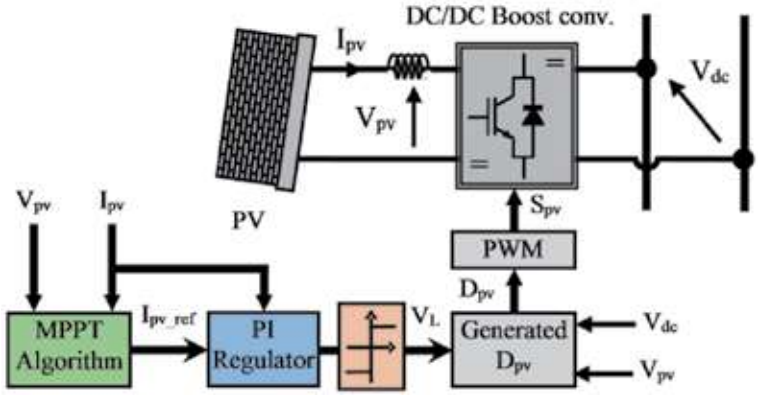

Figure 5.
MPPT algorithm control scheme of PV array.

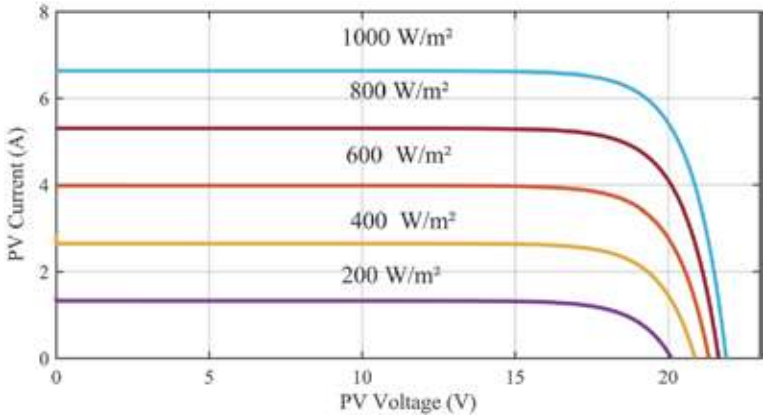

Figure 6.
Typical PV module unit I-V characteristic showing the effects of irradiance.

Figure 6 shows that the PV output power is directly proportional to the irradiance, as in [3, 33]. As such, a smaller irradiance will result in reduced power output from the PV module. However, it is also observed that only the output current is affected by the irradiance. This is expected because the generated current is proportional to the flux of photons.

The number of the PV cell interconnected for the proposed micro-grid is given according to V_{mpp} they result 04 arrays are connected in parallel, each array consists of 27 modules connected in series, each of them delivers 108 W peaks.

3.3 Fuel cell (FC) system modeling and control

The chemical energy of a fuel is directly converting to electrical energy by the PEM FC. The output voltage of a single cell can be defined by Eq. (42), as given in [3, 24, 25]:

$$E_{cell} = E_{Nernst} - E_{Act} - E_{Con} - E_{Ohm} \tag{42}$$

where E_{Con} is the concentration voltage drop, E_{Ohm} is the Ohmic voltage drop, E_{Nernst} is the reversible voltage and E_{Act} is the activation voltage drop. The terminal voltage of PEM fuel cell stacks is defined by Eq. (43), as developed in [2, 3].

$$V_{FC} = N_s E_{Cell} \tag{43}$$

Figure 7 shows voltage and power versus current polarization curves of a PEM FC. It is shown that the activation voltage drop dominates at low current, the Ohmic drop voltage dominates at mid-range current, and the concentration drop voltage dominates at high current. The voltage deviates further as the current is increased, illustrating the effects of drop-voltages. In concentration voltage drop region, the FC output power occurs near the FC rated power.

The FC proper operation is achieved by controlling those auxiliaries, in particular, the air supply system [2–4]. The air consumption system is about 20% of the power supplied by the FC, which reduces the effective capacity of the FC. This is why; the air system control is an important challenge for the development of the FC on micro-grid applications. Indeed, maintaining an adequate level of the oxygen partial pressure in the cathode during rapid variations of FC current in rapid operation mode is important to avoid degradation of the membrane and a decrease in the system efficiency. The excess oxygen ratio control is depicted in **Figure 8**.

Figure 9 shows the FC controller through which the boost converter switch is controlled. Controllers associated with the BBESS and FC are developed in such a fashion that when there is a sudden load power change, the BBESS provides the power instantaneously. In order to make the proper coordination between BBESS

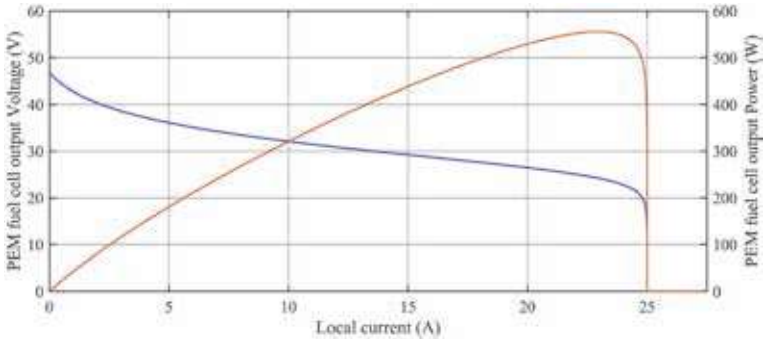

Figure 7.
Power and voltage versus current polarization curves of PEM FC [3].

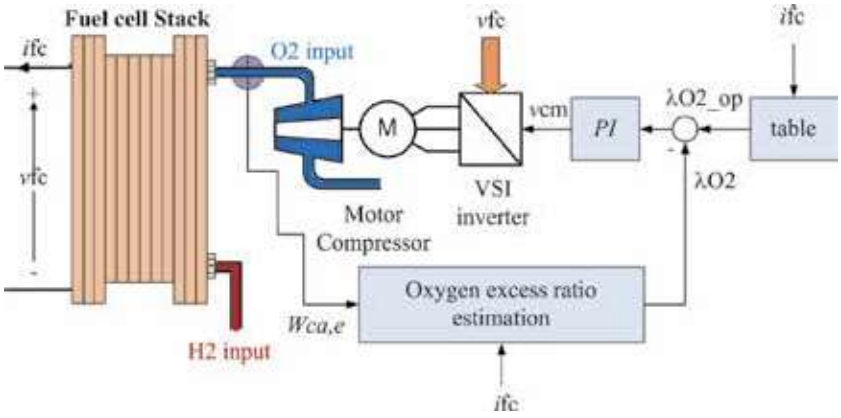

Figure 8.
Excess oxygen ratio control.

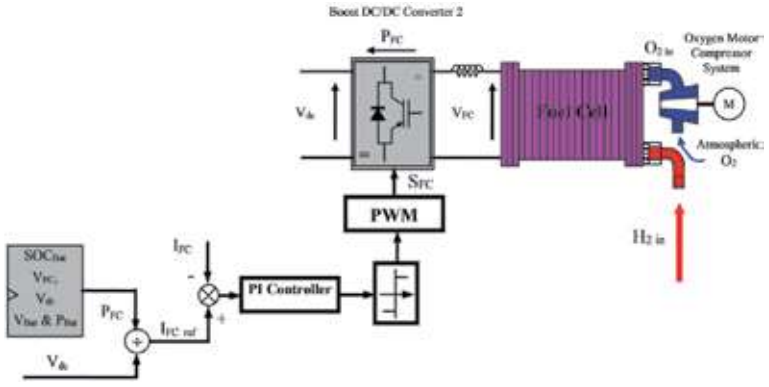

Figure 9.
Boost converter controller associated with fuel cell.

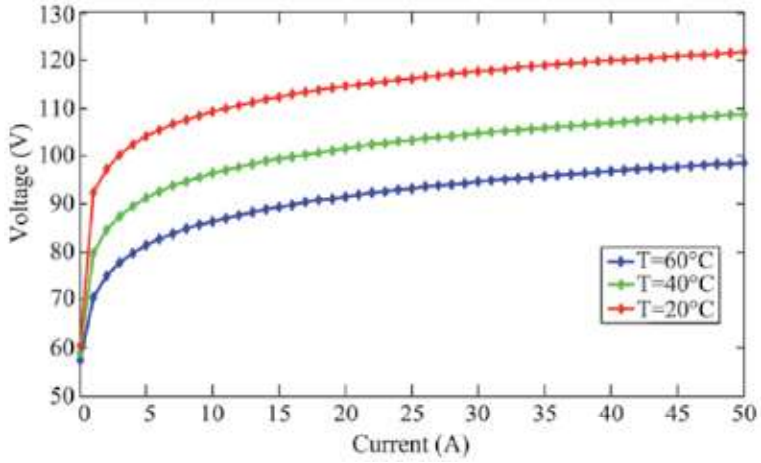

Figure 10.
Typical characteristic of an electrolyzer under different temperatures [3].

and FC, the boost converter controller associated with FC is developed based on assuming BBESS current is ideally zero. Moreover, when SOC of the battery reaches its minimum at 20%, the fuel cell should be generated the required power.

In this work, the PEM fuel cell is composed of 2 × 6 stacks with a power rating of 10 kW.

3.4 Modeling and control of electrolezer system

The water electrolyzer description is presented in [3, 5, 6]. The U(I) electrolyzer model characteristics used in this study at different cell temperatures are shown in **Figure 10**. At a given current, the higher of the operating temperature, the lower is the terminal voltage needed.

The empirical U(I) equation of an electrolyzer cell can be expressed as [3]:

$$U_{cell} = U_{rev} + (r_1 + r_2 T) I_{elect}/A + k \tag{44}$$

$$k = k_{elec} \ln\left(\left(k_{T_1} + k_{T_2}/T + k_{T_3}/T^2\right) I_{elect}/A + 1\right) \tag{45}$$

where U_{cell} is the cell terminal voltage; U_{rev} is the reversible cell voltage; r_1 and r_2 are the parameters for the Ohmic resistances inside the electrolyzer; k_{elec}, k_{T1}, k_{T2}, and k_{T3} are the parameters for the overvoltage; A is the area of the cell electrode; I_{elect} is the electrolyzer current and T is the electrolyzer cell temperature.

The excess energy produced is first pushed into the battery until it reaches its upper limit of charge carrying capacity and then the excess power is fed to the electrolyzer and is regulated via the buck DC/DC converter, as illustrated in **Figure 11**. The decision about switching on the control action is carried out by comparing the upper limit of the battery state of charge (SOC) and the present status of SOC. When the SOC reaches its maximum limit at 80%, the controller will increase the duty cycle as a function of overvoltage in the DC-grid voltage.

3.5 Battery bank (BB) system modeling

In this work, we have implemented a standard battery model, as given in [2–6]. The lead-acid battery is modeled by putting in series an electromotive force corresponding to the open-circuit voltage when it is charged E_{bat}, a capacity

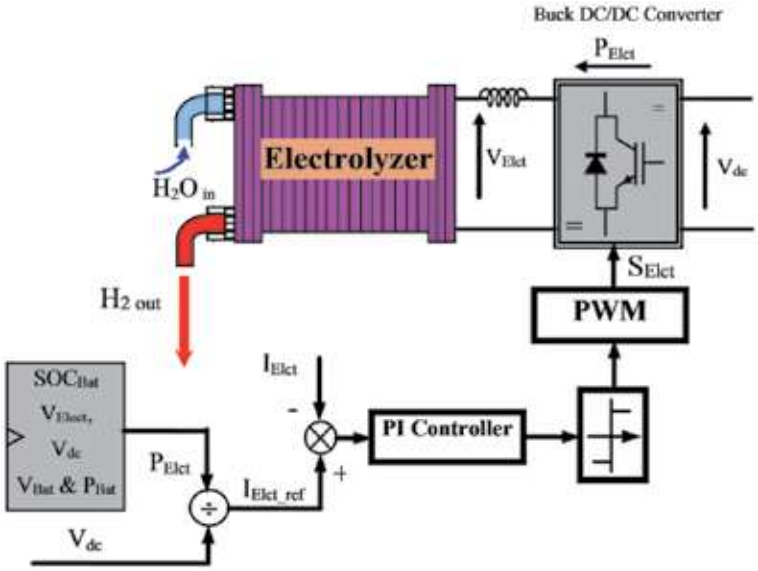

Figure 11.
Buck converter controller associated with an electrolyzer.

indicating the internal capacity of a battery (C_{bat}) and an internal resistance R_{bat}, as illustrated in **Figure 12**.

The battery terminal voltage is given by Eq. (46), as follow:

$$V_{bat} = E_{bat} - R_{bat} \cdot I_{bat} \tag{46}$$

$$E_{bat} = E_0 - V_{cbat} \tag{47}$$

$$V_{cbat} = K_{bat} \cdot \frac{Q}{Q - K_{bat} \cdot \int i_{bat}\, dt} + A_{bat} \cdot \exp\left(-B_{bat} \cdot \int i_{bat}\, dt\right) \tag{48}$$

where E_0 is the no-load battery voltage (V), K_{bat} is the polarization voltage (V), Q is the battery capacity (Ah), A_{bat} is the exponential zone amplitude (V), B_{bat} is the exponential zone time constant inverse $(Ah)^{-1}$, V_{Bat} is the battery voltage (V), R_{bat} is the battery internal resistance (Ω), I_{Bat} is the battery current (A), and $\int i_{bat}\, dt$ is the charge supplied and drawn by the battery (Ah).

The battery state of charge (SOC) is an important parameter to be controlled. It is the amount of electricity stored during the charge; the Q_d is the ampere-hours stored in the battery during a time (t) with a charging current I_{bat} and C_{bat}.

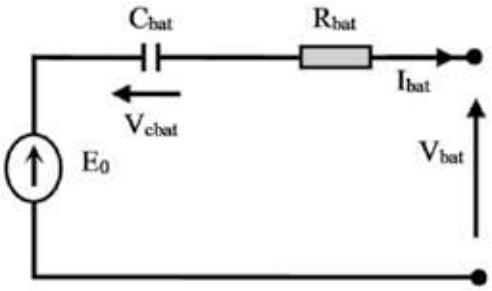

Figure 12.
Electrical model of lead-acid battery.

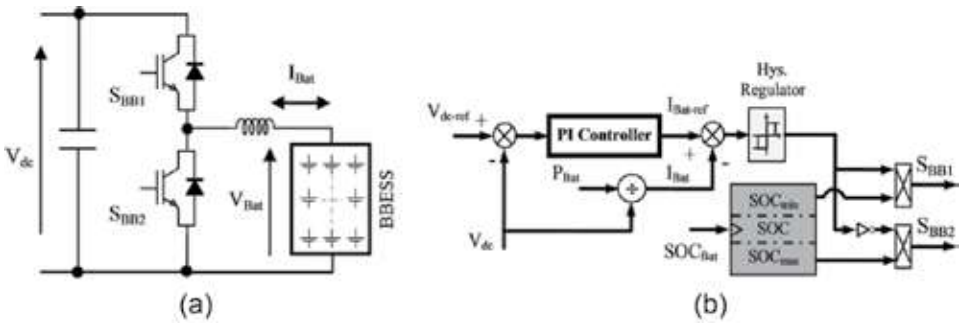

Figure 13.
Schematic diagram of BBDC converter controller associated with BBESS. (a) Power system conversion, and (b) Control system.

The supervisory system must know the battery state of charge to make a decision according to its status and the load power demand.

In case of modern lead acid batteries, charge acceptance is very high; typically, the SOC range is between a low limit around 20% and upper limit around 80% [2–6], where the SOC is given by Eq. (49).

$$SOC(\%) = 100 \cdot \left(1 - \frac{Q_d}{C_{batt}}\right) = 100 \cdot \left(1 - \frac{I_{batt} \cdot t}{C_{batt}}\right) \tag{49}$$

The primary objective of the Buck-Boost DC converter (BBDC) control is to maintain constant DC-grid voltage, as a reference value, and to discharge/charge power from/into BBESS according to the required power. The schematic diagram of the BBESS Buck-Boost DC converter and its control are presented in **Figure 13**. The BBESS voltage can be kept lower as compared to the DC-grid voltage reference ($V_{dc\text{-}ref}$) using BBDC. Hence, several batteries are required to be connected in serial. In the proposed micro-grid, the V_{bat} is kept around 420 V. Therefore, it is required that 36 cells of batteries are connected in series.

3.6 Energy management system

The BBESS can act either as a power supply or as a dump load, it's should discharge/charge within specified limits when there is deficit/surplus of hybrid power, due to the weather conditions or perturbation in power requirement. Knowing that, due to BBESS dynamics, it cannot feed the power instantaneously and hence unable to stabilize the DC-grid voltage during transient state. In order to overcome this constraint, a FC is incorporated using a Boost converter (connected between FC and DC-grid), as given in **Figure 9**, in such a manner that the FC provides the power instantaneously. Consequently, this FC should increase the BBESS power which is decreasing. The flow chart of the above-discussed control coordination among various sources is depicted in **Figure 14**.

The DC-grid control voltage is assured by the Buck-Boost DC converter associated with BBESS, as illustrated in **Figure 13**. The BBESS reference power is given by the power flow available in the DC-grid while respecting the flowchart given in **Figure 14**, imposed by the energy management system proposed.

The different powers which flow between the generation sources, the storage systems and the required demand are calculated as:

$$P_g = P_{AC} = P_{L-AC} + P_{gAC} \tag{50}$$

$$P_{rAC} = P_g - P_s \tag{51}$$

$$P_{rg} = P_{L-DC} + P_{rAC} \tag{52}$$

$$P_{Net} = P_r + P_{rg} \tag{53}$$

$$P_{FC} = P_{Net} - P_{Bat} - P_{Elect} \tag{54}$$

where, P_s and P_r are the stator and rotor powers generated by DFIG. The $P_{L\text{-}AC}$ and $P_{L\text{-}DC}$ are the variable AC and DC load powers, P_{rAC} is the power transferred through DC/AC converter II, P_{Elc} and P_{Bat} are the Electrolyzer and BBESS powers, also P_{FC} and P_{pv} are the generated FC and photovoltaic powers, respectively. Whereas P_{AC} and P_g are the powers exchanged between the proposed micro_grid system and the AC grid, P_{gAC} is the power exchanged between the proposed MG associated with its local variable AC load and the external AC grid.

The energy control and management strategies consist that, at any given time, the BBESS provides the averaged power and the FC provides the instantaneous power. When the BBESS SOC is reached its maximum at 80% in charge mode, the electrolyzer is turned on to store the excess power and to begin producing hydrogen, as given in **Figure 11**, which is delivered to the hydrogen storage tanks, as shown in **Figure 1**, but if this limit is reached its minimum at 20% in discharge mode, the FC provides the deficit required power. However, in case of a high wind or solar energies conditions or lower demand ($P_{Net} > 0$), the surplus power at first is supplied to the BBESS until it reaches its upper limit of charge carrying capacity, the Electrolyzer is used to support the BBESS operations to absorb the additional power, as given in **Figure 14**.

In case of low or no power generation from RESs and even high demand ($P_{Net} < 0$), the power requirement will be supplied by the BBESS up to SOC lower limit. At this moment, the FC ensures continuity of service by supplying the power requirement.

The DC-grid voltage control by the Buck-Boost actually means managing the flow of available power at this DC-grid, while respecting the flowchart given in **Figure 14**, imposed by the energy management system proposed.

The local reactive power compensation exchanged between the proposed MG and the bus-bar from the AC side (AC grid), Q_{AC} or Q_g, is provided by the DFIG. Knowing that, the reactive power at the DC/AC converter II output is forced to zero (operating at unity power factor).

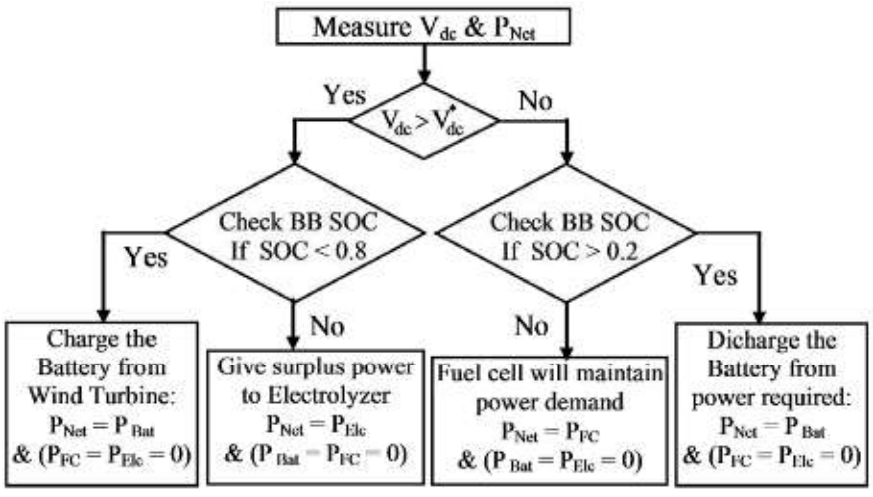

Figure 14.
Flowchart of control coordination and energy management algorithm.

$$Q_{AC} = Q_g = Q_s + Q_{rAC};\ Q_{rAC} = 0 \tag{55}$$

$$Q_{AC} = Q_s = Q_g = Q_{gAC} + Q_{L-AC} \tag{56}$$

$$Q_{L-AC} = P_{L-AC} \cdot tg(\varphi_{L-AC}) \tag{57}$$

where, Q_s is the reactive power flowing between the DFIG stator and the AC grid side. While, $Q_{L\text{-}AC}$ and Q_{AC} or Q_g represent respectively, the reactive powers exchanged with the local AC load and the AC grid together with the proposed system. Q_{rg} is the reactive power transferred through DC/AC converter II. The local load phase shift is given by φ_{L-AC}, where P_{gAC} is the power exchanged between the proposed MG associated with its local variable AC load and the external AC grid.

4. Simulation results and discussion

In this section, the WT-DFIG control simulation and the utility of the proposed MG simulation have been presented.

4.1 WT-DFIG control simulation results and discussion

In this section, the simulation of the Variable Wind speed generator (VSWG) behavior using DFIG in conjunction with an indirect AC-AC converter connected to the grid is developed. So, in order to test the control efficiency and robustness of the WT-DFIG under constraints reflecting an operation that is close to its actual behavior, we opted for the wind speed profile illustrated in **Figure 15a**. In the aim to take advantage and to verify the validity and highlight of the proposed system performances, a model allowing the machine with its control behavior simulation, for different operating zones, is developed, as illustrated in **Figure 4**.

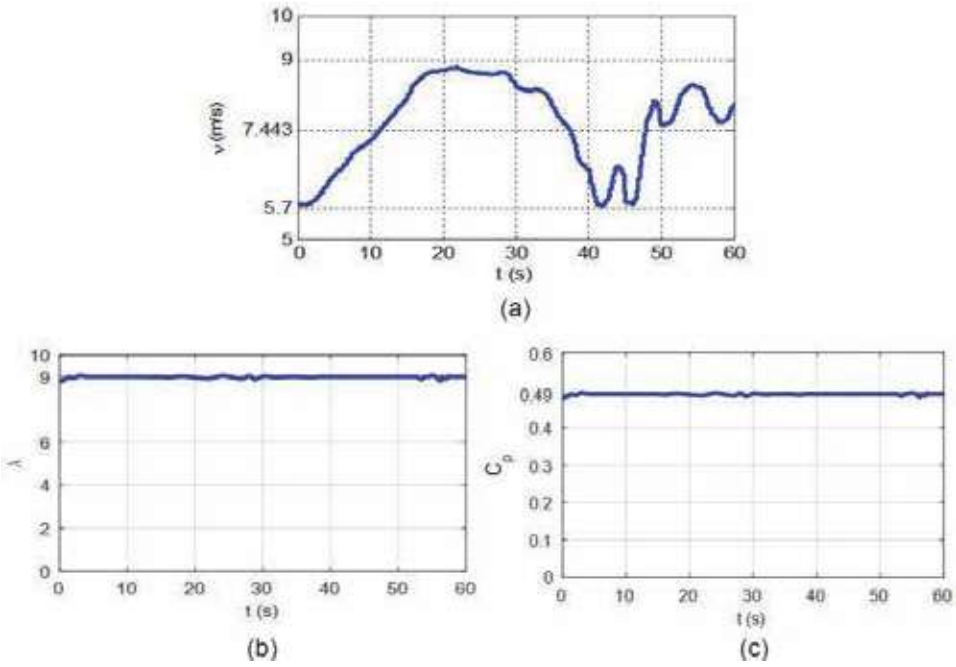

Figure 15.
Waveforms of WT characteristics: (a) wind speed profile. (b) Tip-speed ratio. (c) Power coefficient.

The machine and control parameters details considered in this studied are given in [3, 19], where the simulation results are presented thereafter, as illustrated in **Figures 15–22**.

The MPPT algorithm applied makes it possible to have the ratio of speed equal to its optimum value (λ_{opt} = 9) with a maximum power coefficient ($C_{p\text{-}max}$ = 0.49) as indicated in **Figure 15b** and **c**. These last variables are almost constant despite the fluctuations caused by the wind speed profile variations.

The results illustrated in this section show that the references tracking is very well achieved, which is verified for the two variables, the active power delivered to

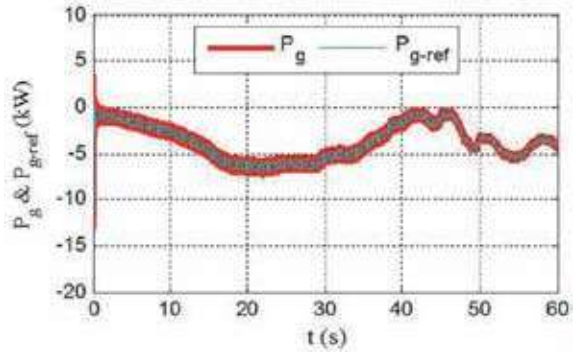

Figure 16.
Total active power generated by the WT-DFIG.

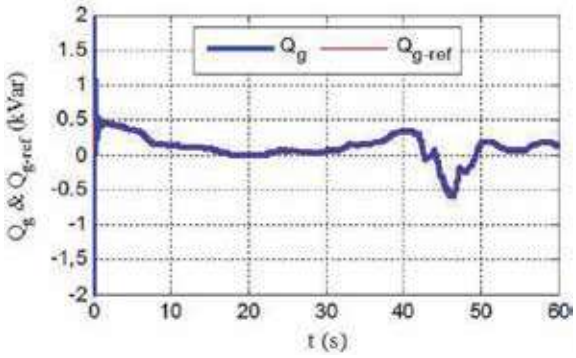

Figure 17.
Total reactive power compensated by the DFIG.

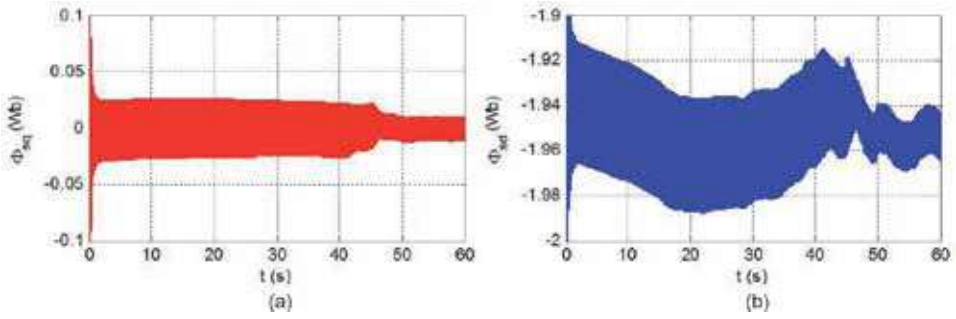

Figure 18.
DFIG direct and quadrature stator flux. (a) Direct stator flux. (b) Quadrature stator flux.

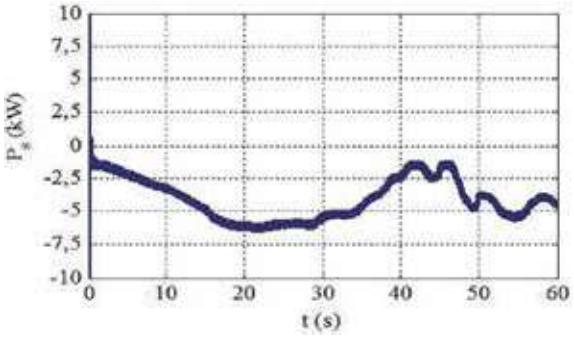

Figure 19.
Active power generated by the DFIG stator.

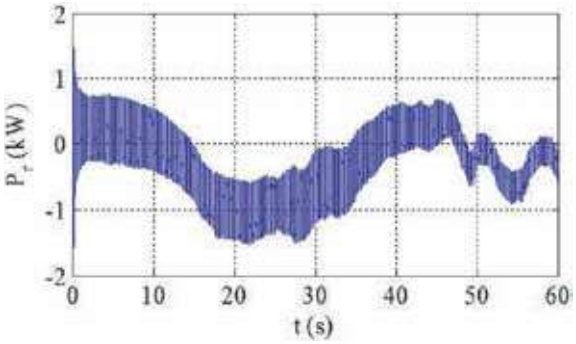

Figure 20.
DFIG rotor active power.

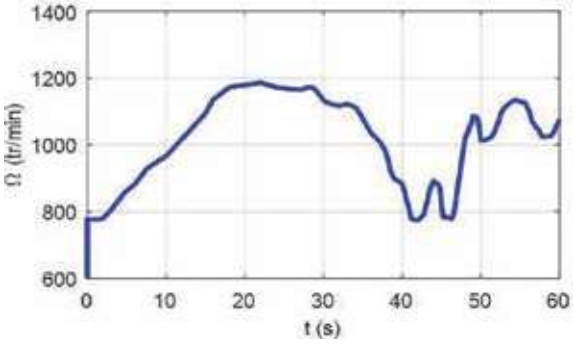

Figure 21.
DFIG mechanical speed.

the AC grid and the local reactive power to be compensated, as illustrated in **Figures 16** and **17**.

In addition, the control decoupling is represented on the stator flux evolution, as given in **Figure 18**; where, the quadrature component is always kept zero (**Figure 18a**), while that of direct axis follows the form of the active power produced, as presented in **Figures 18b** and **19**.

The machine operates in the three operation modes, as shown in **Figures 20–22**. For $s > 0$, the DFIG is run in the sub-synchronous mode, indicating that the rotor power is supplied by the grid. For $s < 0$, the DFIG is operated in the

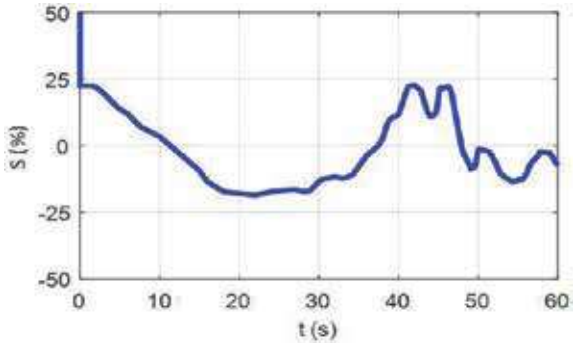

Figure 22.
DFIG slip.

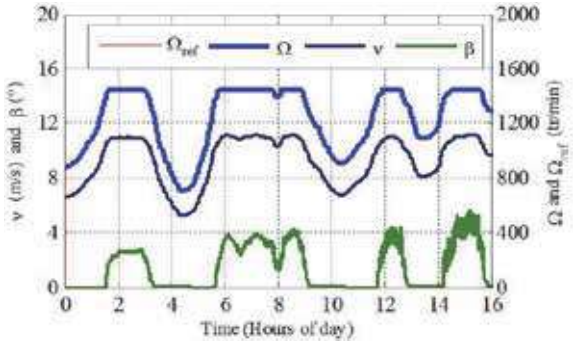

Figure 23.
Wind speed profiles, DFIG mechanical speed with its reference with blade pitch angle evolution.

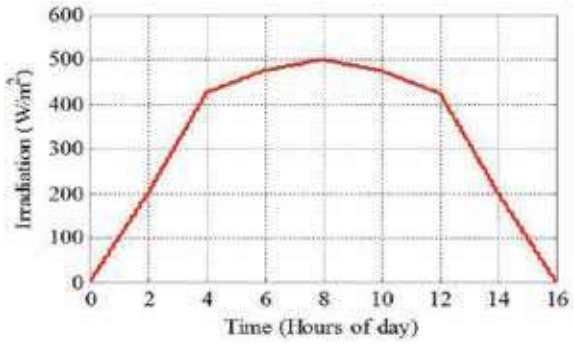

Figure 24.
Irradiation profiles waveform.

super-synchronous mode. It can be seen, from **Figure 21**, that the rotor power flow direction is reversed. For s = 0, the DFIG functions as a synchronized asynchronous generator, the rotor active power is absorbed as rotor Joules losses.

4.2 Global MG control simulation results and discussion

In this part, the analysis of the performances and behavior of the proposed MG, as presented in **Figure 1**, will be studied. The proposed system simulation is realized

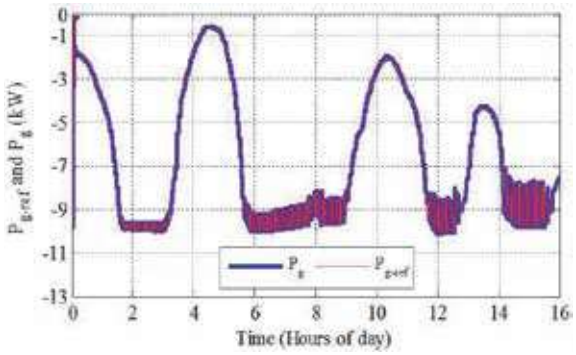

Figure 25.
WT-DFIG generated active power evolution with its reference.

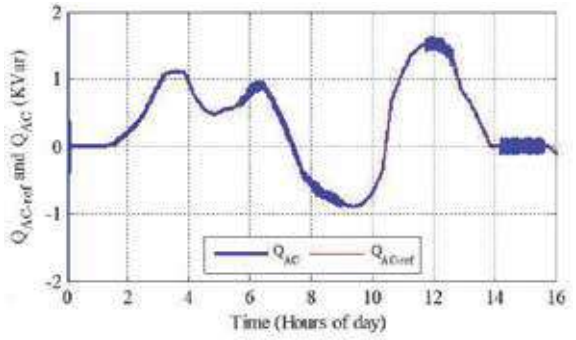

Figure 26.
Evolution of the reactive power compensation with its reference.

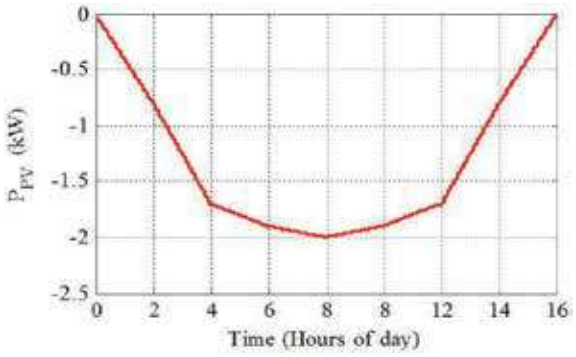

Figure 27.
Evolution of the PV power generation.

under different situations, as variable load demand and random weather conditions data (wind speed, solar irradiance, etc.). The wind speed profile is selected shown the two useful zones operating ranges of the turbine, as given in **Figure 2**. In zones I and II, the maximum power extraction algorithm (MPPT) is applied, but in zone III, defined as over-speed turbine operations, constant power is generated by acting on the pitch angle control, as illustrated in **Figure 23**. Simulation results for this case are given and discussed in the following section, as illustrated in **Figures 23–32**.

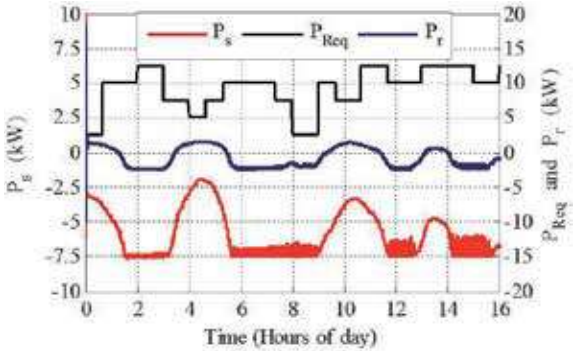

Figure 28.
Average required demand power and the stator active power generated by DFIG with its rotor active power.

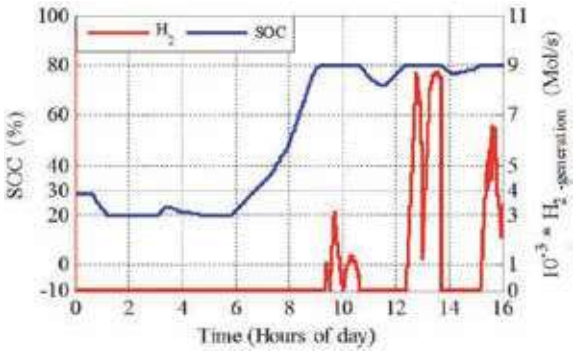

Figure 29.
Waveforms of the hydrogen (H_2) generation rate and the battery SOC evolution.

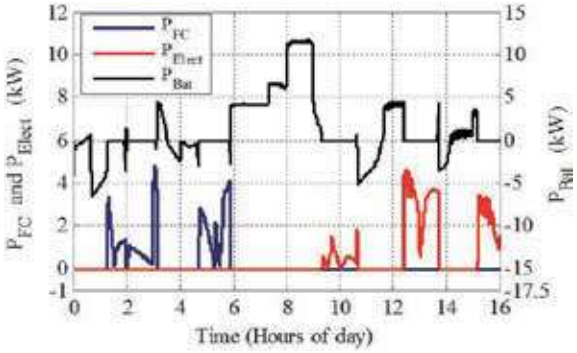

Figure 30.
Evolution of the hybrid storage powers (power available for H_2 generation and BBESS power) and FC generated power.

The simulation parameters of the different elements composing the proposed system, associated controls and proposed energy management are given in [2, 3, 19].

The total hourly averages of the weather data (solar radiation and wind speed profile) and powers required profiles, over 16 hours by day are shown in **Figures 23** and **24**. The wind speed profile is chosen in a manner that the WT-DFIG operates in a different area (MPPT and blade pitch control zone), as presented in **Figure 23**.

Also, this figure illustrates the blade pitch angle. When the generated stator active power reached its maximum value (P_{smax}), the pitch angle control is activated, it generates the variation of the tip speed ratio and the power coefficient. The DFIG mechanical speed is kept constant, at its rated value, as shown in **Figure 23**. However, in the MPPT regions, the produced active power is maximized. Where the blade pitch angle, tip speed ratio and the power coefficient are maintained at constant value ($\beta = 0$, $\lambda = \lambda_{opt} = 9$, $C_p = C_{p\text{-}max} = 0.49$).

The waveform of the generator mechanical speed is depicted in **Figure 23**, where the generated grid active power and the local reactive power compensation are illustrated in **Figures 25** and **26**, respectively. These results affirm that the good performances of the proposed control, where the generated grid active power varies as a result of the wind speed profile to maximize the power coefficient in the MPPT zones. While in the blade pitch control, the generated power (**Figure 25**) is constant to maintain the constant electromagnetic torque, whereas, the compensated reactive power is kept at its reference and varies according to the magnitude of the direct stator flux. Thus, the WT is used in an optimal way and justifying the usefulness of the DFIG in the possibility of management and the active-reactive powers control.

Figures 27 and **28** show that all the same of changes in the power distribution curve of generated solar power (**Figure 27**), stator active power generated by DFIG with its rotor active power and the required power (**Figure 28**).

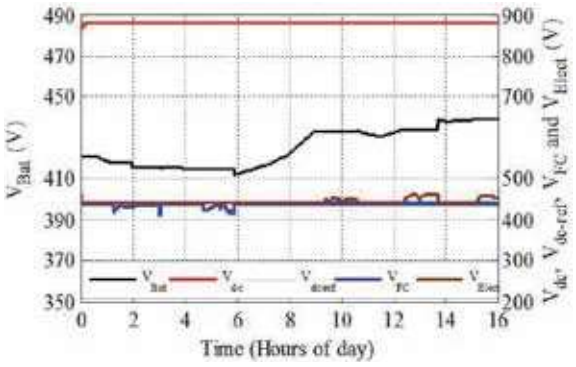

Figure 31.
Evolution of the DC-grid, electrolyzer, battery and FC voltages waveforms.

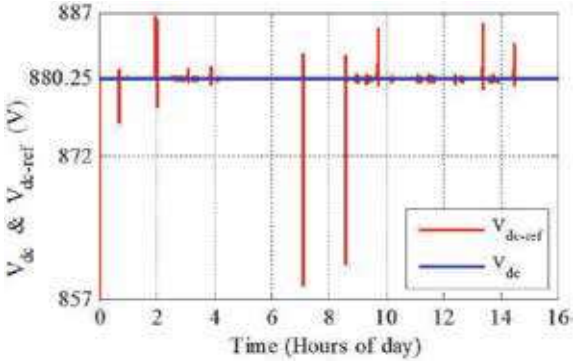

Figure 32.
Zoom of the DC-grid voltage evolution with its reference.

The waveforms of the battery SOC and the H_2 generation rate over are shown in **Figure 29**. The SOC is limited within range (20–80%).

Hence, **Figures 29** and **30** show when the generation powers are insufficient to supply the required power and the SOC of the battery reach its minimum at 20%, the FC supplements the deficit energy to meet the demand requirement. While, when the generated power is greater than the required demand and the battery is fully charged, the SOC reaches its maximum limit at 80%, the excess energy is used to generate the H_2, as illustrated in **Figure 29**.

Figure 31 shows that the FC, the Electrolyzer, the battery bank and the DC-grid output voltage variations are respectively expected. Indeed, the evolution of the different voltages represented in this figure follow the evolution of the power transited by the element that represents. In addition, the reference tracking of the DC-grid voltage is depicted in **Figure 32**. This voltage is constant and follows its reference, despite the variations in hybrid powers generation and required demand. So, it can be confirmed that the performances of the buck-boost DC-DC bidirectional converter controller are quite satisfactory in both transient and steady-state hybrid power and required demand conditions.

5. Conclusions

In this paper, a renewable multi-source microgrid associated with a hybrid energy storage system is studied. The energy sources combined WT-DFIG with a PV generator and a Fuel cell. Whereas, the hybrid energy storage is composed of batteries bank energy storage system (BBESS) associated with an electrolyzer system, which is a hydrogen generator.

The simulation model of the overall hybrid MG system has been developed using MATLAB/Simulink.

The system configuration and the characteristics of the main components in the system are given, and the overall control and power management strategy for the proposed hybrid energy system is presented. The WT-DFIG and PV generation systems are the main power generation devices and the electrolyzer-BB act as a dump load using any excess power available to BB charging and produce H_2. The FC and BB system is the backup generation and supply power to the system when there is a power deficit.

The obtained results confirm also the robustness and the efficiency of the proposed control that allows us to enjoy the benefits of the combination between a stator flux-oriented control (SFOC) with variable structure control (VSC) process, using the nonlinear Sliding Mode control (SMC) technique to control the generated active power to the AC grid and to govern the local reactive energy compensation. This latter justifies the usefulness of the DFIG in the possibility of management and the active-reactive powers control, especially, operating as a local reactive power compensator, where it can work in the synchronized asynchronous mode as a synchronous generator.

Furthermore, the obtained results showed clearly the satisfactory performances and the effectiveness of the proposed micro-grid. Indeed, the main objectives of this contribution, which are: efficient control of the coordination between the various energy sources, a proper operation of the proposed micro-grid (DC and AC grid) providing a better energy quality and an uninterrupted service are satisfied. Then, better energy management is observed, permitting an optimal operation of the whole system with high performances of the micro-grid under unfavorable and critical conditions such as power required demand variations and random weather conditions data (wind speed random profile, variable solar irradiance).

Author details

Salah Tamalouzt[1]*, Nabil Benyahia[2], Abdelmounaim Tounzi[3] and Amar Bousbaine[4]

1 Laboratory LTII, Faculty of Technology, University of Bejaia, Algeria

2 Laboratory LATAGE, University M/Mammeri of Tizi-Ouzou, Algeria

3 Laboratory L2EP, University of Lille, Lille, France

4 College of Engineering and Technology, University of Derby, UK

*Address all correspondence to: tamalouztsalah@yahoo.fr